Available online at www.sciencedirect.com

ScienceDirect

Scripta Materialia 104 (2015) 67–70

Scripta MATERIALIA

www.elsevier.com/locate/scriptamat

The role of C and Mn at the austenite/pearlite reaction front during non-steady-state pearlite growth in a Fe–C–Mn steel

M.M. Aranda,[a,*] R. Rementeria,[a] J. Poplawsky,[b] E. Urones-Garrote[c] and C. Capdevila[a]

[a] *Materalia Research Group, Centro Nacional de Investigaciones Metalúrgicas (CENIM-CSIC), Avda. Gregorio del Amo, 8, 28040 Madrid, Spain*

[b] *Center for Nanophase Materials Sciences, Oak Ridge National Laboratory, PO Box 2008 MS 6064, Oak Ridge, TN 37831-6064, USA*

[c] *Centro Nacional de Microscopía Electrónica (CNME), Facultad de Ciencias Químicas, Universidad Complutense de Madrid, Avda. Complutense s/n, 28040 Madrid, Spain*

Received 13 February 2015; revised 6 April 2015; accepted 7 April 2015
Available online 18 April 2015

The role of C and Mn during the growth of pearlite under non-steady state conditions is analyzed by comparing phase compositions of austenite, ferrite and cementite ($\gamma+\alpha+\theta$) through the use of transmission electron microscopy (TEM), energy dispersive X-ray spectroscopy (EDS), and atom probe tomography (APT) measurements across the austenite/pearlite interface.
A local Mn enrichment and C depletion at the austenite/pearlite interface has been measured, which causes a change in the transformation driving force with time during divergent pearlite growth.

Keywords: Divergent pearlite; Interface diffusion; Growth rate; Pearlitic steel

Divergent pearlite is a kind of pearlite whose key features are a decreasing growth rate and an increasing interlamellar spacing as a function of reaction time. These observations were attributed to a continuously changing carbon concentration ahead of the reaction front when reaction proceeds [1]. Cahn and Hagel [2] first reported this unusual structural feature in a Fe–C–Mn steel, that provided new insights on the influence of composition during the pearlite transformation. They named this variant divergent pearlite, as opposed to the time-invariant behavior observed in plain-carbon steels (constant pearlite).

In an attempt to explain the results of Cahn and Hagel, Hillert [1] described divergent pearlite as an ortho-pearlite structure formed under a redistribution of Mn between ferrite and cementite. The reaction of divergent pearlite is observed when the composition of the parent austenite is located within the ($\gamma+\alpha+\theta$) three-phase region. The fact that the austenite reaches the equilibrium composition different from the bulk composition leads to a continuous change of austenite composition causing a reduction in the driving force for this transformation. As a result, the interlamellar spacing increases and the growth rate decreases with reaction time until austenite reaches equilibrium.

According to Hillert [1], in order to examine the conditions at the austenite/pearlite interface, it should be a sensible approach to assume in a Fe–C–Mn steel, that the growth rate is slow enough such that there is sufficient time for C to establish a uniform activity along the pearlite–austenite interface. The intersection points of the C isoactivity line that passes through the bulk composition (indicated as ac_{t0} in Figure 1) with the $\gamma/(\gamma+\alpha)$ and $\gamma/(\gamma+\theta)$ extrapolated phase boundaries represent the composition of austenite at the ferrite and cementite interfaces at the beginning of the transformation.

The end of the tie lines (red lines in Figure 1) corresponding with these intersections would give the corresponding composition of the growing ferrite and cementite. The composition of the growing pearlite lies on the straight line joining these two points (indicated by the solid gray line). Since the Mn diffusivity at the transformation temperature is very slow, it is sensible to consider that Mn contents of the bulk composition and the growing pearlite (indicated by the solid gray symbol) are the same. Therefore, the growing pearlite has a higher C content than the alloy, and hence, it draws C from the parent austenite leaving a C-depleted zone. This leads to a reduction in the activity of C in the vicinity of the interface. As the transformation progresses, the LE conditions prevailing at the interface change continuously, and can be described by C isoactivity lines corresponding to lower C activities

* Corresponding author.

http://dx.doi.org/10.1016/j.scriptamat.2015.04.005
1359-6462/

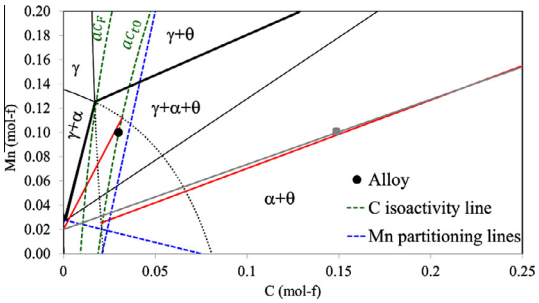

Figure 1. Isothermal section at 600 °C for the Fe–C–Mn system. The alloy (black circle) is located within the three phase region. The dotted lines are the extrapolated $\gamma + \alpha$ and $\gamma + \theta$ phase boundaries, and the blue lines are the partitioning-no partitioning boundaries for α and θ. (For interpretation of the references to color in this figure legend, the reader is referred to the web version of this article.)

moving to the left (indicated as ac_F) until the corner of the stable γ phase field is reached. The equilibrium compositions for ferrite and cementite are given by the black solid lines in three phase region.

The LE Mn content of the growing ferrite and cementite increases in accordance with the variation in the operative tie-lines as the reaction proceeds. Thus, the Mn concentration difference in the γ at the γ/α and γ/θ interfaces, which drives the lateral Mn redistribution, decreases as growth proceeds, and this diminished driving force results in an increasing interlamellar spacing and a decreasing growth rate [3].

Hutchinson et al. [3] investigated the growth of partitioned pearlite and the interfacial conditions governing pearlite growth by comparing analytical transmission electron microscopy (TEM) measurements and theoretical values obtained by Thermocalc software relying on the work of Hillert as a theoretical basis. However, there was no previous experimental work on an examination varying austenite local conditions during reaction time.

Therefore, the goal of this paper is to determine the local composition of austenite at different reaction times to seek the above mentioned Mn and C gradients. In order to demonstrate conclusively that Mn diffusion in austenite is slow enough to produce a Mn-enriched and C-depleted zone in austenite, atom probe tomography (APT) measurements across the austenite/pearlite interface are presented.

The nominal composition of the studied steel is Fe–2.98C–9.66Mn (at.%). Isothermal heat treatments for various times (3, 6, 18 and 36 h) were designed with the Thermocalc software package and the TCFE7 database in order to select a temperature at which divergent pearlite can be expected. As illustrated by the isothermal section for 600 °C shown in Figure 1, the alloy is located within the (γ+α+θ) three phase field region.

Samples for scanning electron microscopy (SEM) and TEM examination were prepared following standard methods as described elsewhere [4,5]. A JEOL 3000F TEM equipped with an Oxford INCA energy dispersive X-ray spectrometer (EDS) system was used for the analytical electron microscopy (AEM) measurements across the austenite/pearlite interface. The EDS measurements were quantified by the Cliff–Lorimer ratio method. Furthermore, APT analysis was performed on the austenite/pearlite interfaces machined by top-down and cross-sectional FIB lift-out methods described by [6,7] in a FEI Nova 200 dual beam SEM/focused ion beam (FIB) miller. APT analyses were performed in voltage and laser mode at 200 kHz using the ORNL local electrode atom probes, CAMECA Instruments, Inc. LEAP® 2017 and 4000× HR, respectively. Voltage mode runs were performed at 50 K with a 20% pulse fraction, while laser mode runs were performed at 30 K with a 50 pJ laser power. A lower pulse energy was used to mitigate large C molecular evaporation.

The standard method for determining growth rate, namely the maximum nodule radius method [8], presents some limitations, and therefore, the pearlitic growth rate was measured according to the procedure described in [2]. The microstructure and the growth kinetics observed for the alloy transformed at 600 °C for different isothermal times (18 and 36 h) are shown in Figure 2a and b, respectively.

As in the case of growth rate, traditional methods for interlamellar spacing, σ_0, measurements [9] are not adequate for samples with a variable interlamellar spacing across the nodule or over time because they provide an average interlamellar spacing value neglecting divergency.

For this purpose, the analysis using SEM images was performed as follows. First, a straight line is drawn from the prior austenite grain boundary ($x = 0$) to the reaction front ($x = R_{max}$), as illustrated in Figure 2a. The interlamellar spacing variation along this line is then evaluated by measuring the number of interceptions with cementite of the superimposed random lines perpendicular to R_{max}. Dividing the length of each perpendicular line by the number of interceptions, the interlamellar spacing is estimated.

Since growth rate varies over time, it is necessary to measure the interlamellar spacing as a function of time. The variation of the pearlitic interlamellar spacing across the pearlitic nodule for two different times is shown in Figure 2c. The interlamellar spacing becomes larger closer to the reaction front. From Figure 2b and c, it might be concluded that pearlite grows under non-steady-state conditions and that lamellar divergence is more pronounced for longer times.

A detailed austenite/pearlite interface composition analysis was performed to determine the Mn and C concentration profiles across the γ/α and γ/θ growth interfaces as a function of time in order to establish if LE conditions are fulfilled during pearlite growth. Figure 3a and b shows two interfaces at two different holding times in which the profiles across the interface are labeled.

AEM results of Mn redistribution profiles across the relevant interfaces are shown in Figure 3c and d. The Mn values in both ferrite and cementite reported in Figure 3c and d are the average of 2–3 interfaces, where 10 individual measurements were done along the mid rib of a lamella, and the error bars correspond to the standard deviation of these measurements. Theoretical LE and full equilibrium values predicted by Thermocalc are plotted for cementite and ferrite (dashed line and solid line shown in Figure 3c and d), indicating that at the early stages of pearlite transformation, LE conditions prevail at the interface. As decomposition time progresses, the Mn concentration in both cementite (red points in Figure 3c) and ferrite (blue points in Figure 3d) is continuously increasing during the pearlite growth. As a result, the LE interfacial compositions at the pearlite/austenite interface change with time. These results are in good agreement with other research [3] regarding the interface composition in divergent pearlite, and are therefore consistent with growth under non-steady-state conditions.

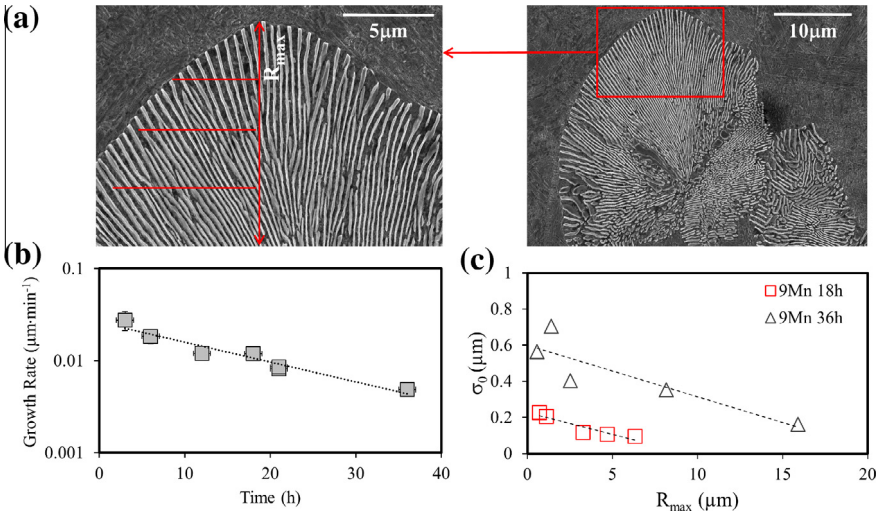

Figure 2. (a) SEM images showing interlamellar spacing for the studied alloy after 18 h of isothermal treatment at 600 °C. (b) Evolution of the pearlitic growth rate at 600 °C. (c) Interlamellar spacing variation across the pearlitic nodule after 18 and 36 h of decomposition.

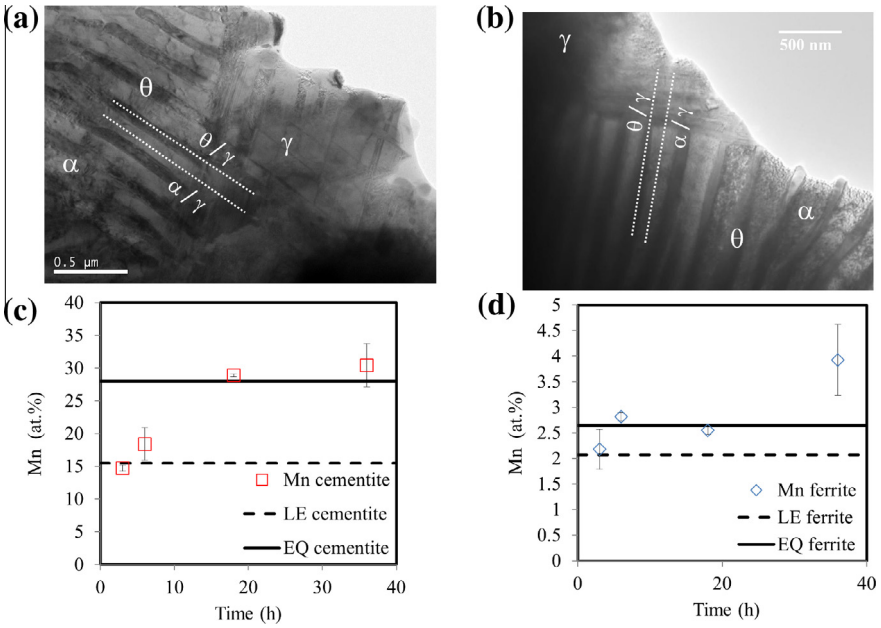

Figure 3. TEM images and EDS profiles across the austenite/pearlite interface after 600 °C isothermal holdings of (a) 3 h and (b) 18 h. AEM measurements of Mn concentration vs. decomposition time in (c) cementite and (d) ferrite during divergent pearlite formation.

For the purpose of characterizing the initial and the final states of the austenite in contact with ferrite and cementite during transformation, APT was used to determine the Mn and C concentration profiles in the vicinity of the pearlite growth front. This, coupled with thermodynamic calculations, enlightens the roles of Mn and C in accounting for the non-steady state growth rate. The APT needle-shaped specimen, (Fig. 4)a, was fabricated in such a way that all three phases were present in the same volume of analysis. Concentration isosurfaces were generated within regions of interest only containing the γ/α and γ/θ interfaces such that the proximity histograms were only across the interfaces of interest.

Proximity histograms across the concentration isosurfaces corresponding to the γ/α and γ/θ growth interfaces after isothermal decomposition at 600 °C for 6 h are shown in Figure 4b and c. As expected, there is a localized spike in C and Mn content along the austenite–pearlite interface due to the PLE mechanism. However, the main focus of this study is the Mn and C contents within the growth front, which are a few nanometers away from the interface. From these results, the Mn values for ferrite and cementite are between the theoretical LE and equilibrium values, and are in good agreement with results obtained by TEM–EDS (Fig. 3). Concerning the austenite composition in contact with ferrite and cementite after 6 h at 600 °C, a local Mn enrichment (10.1 ± 0.4 at.%) and a local C depletion (2.8 ± 0.4 at.%) are observed in the reaction front.

The same analysis was performed after 18 and 36 h of isothermal decomposition. In these cases, the Mn values in the austenite in contact with the growing pearlite were higher than those obtained for 6 h, and the C depletion in

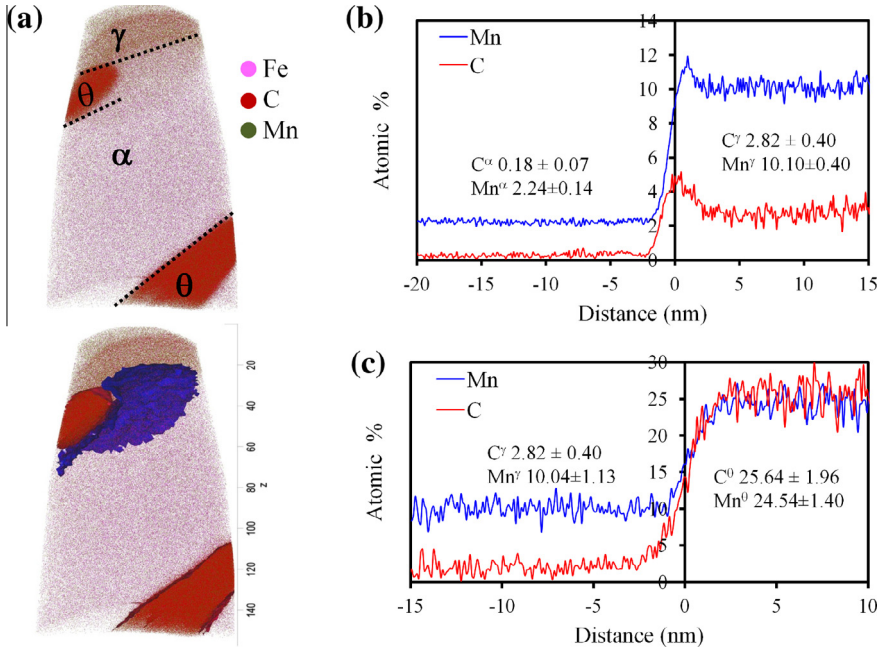

Figure 4. (a) Volume analyzed by APT showing austenite/pearlite interface after aging 6 h at 600 °C, and the concentration isosurfaces from which the proximity histograms were obtained. Mn and C concentrations across the (b) austenite/ferrite interface and (c) austenite/cementite interface.

Table 1. C and Mn concentrations (in at.%) for the as-received state and for austenite, ferrite and cementite phases during pearlite transformation at the reaction front.

	C^{γ}	Mn^{γ}	Mn^{α}	Mn^{θ}
Nominal composition	2.98 ± 0.07	9.66 ± 0.01		
After 6 h	2.8 ± 0.4	10.1 ± 0.4	2.24 ± 0.14	24.54 ± 1.40
After 18 h	2.32 ± 0.14	10.97 ± 0.17	2.31 ± 0.03	27.72 ± 0.04
After 36 h	2.08 ± 0.01	11.17 ± 0.02	2.50 ± 0.11	27.32 ± 0.03

austenite was more significant. The APT measurements for C and Mn concentrations at the austenite in the reaction front (C^{γ}, Mn^{γ}) and the Mn concentration values for ferrite and cementite across the austenite/pearlite interface (Mn^{α} and Mn^{θ}) are summarized in Table 1.

As the C content of the matrix decreases, the isoactivity line describing the conditions at the interface will shift further to the left, and there will be an accompanying change in interfacial compositions to satisfy LE. The end result is a continuous variation of the austenite composition until it reaches the equilibrium with ferrite and cementite. To compensate for this reduction in the C isoactivity, the interlamellar spacing increases (initiating divergency) and the growth rate decreased with reaction time.

In summary, the pearlite grown in the ($\gamma+\alpha+\theta$) field exhibits an increasing lamellar spacing and a decreasing growth rate with time. The associated analytical TEM data, as well as APT measurements across the austenite/pearlite interface, show that the Mn content in the ferrite and cementite phases increases during the growth period. It can also be concluded that LE conditions prevailing at the interface during divergent pearlite transformation change over time until austenite equilibrium with ferrite and cementite is reached.

The authors acknowledge Acerinox for manufacturing the steel. This research was supported by ORNL's Center for Nanophase Materials Sciences (CNMS), which is a U.S. Department of Energy, Office of Science User Facility. Authors acknowledge financial support to MINECO and FEDER in the form of ENE2009-13766-C04-01 and MAT2013-47460-C5-2-P projects.

[1] M. Hillert, Analysis of the effect of alloying elements on the pearlite reaction, in: I. Aaronson Hubert, E. Laughlin David, F. Sekerka Robert, C.M. Wayman (Eds.), TMS-AIME, 1982, pp. 789–806.
[2] J.W. Cahn, W.G. Hagel, Acta Metall. 11 (1963) 561–574.
[3] C.R. Hutchinson, R.E. Hackenberg, G.J. Shiflet, Acta Mater. 52 (2004) 3565–3585.
[4] M.M. Aranda, B. Kim, R. Rementeria, C. Capdevila, C.G. de Andrés, Metall. Mater. Trans. A 45 (2014) 1778–1786.
[5] F.G. Caballero, C. García De Andrés, C. Capdevila, Mater. Charact. 45 (2000) 111–116.
[6] M.K. Miller, G.D.W. Smith, Met. Sci. 11 (1977) 249–253.
[7] Michael K. Miller, R.G. Forbes, Atom-Probe Tomography: The Local Electrode Atom Probe, Springer, New York, NY, 2014.
[8] R.F. Mehl, W.C. Hagel, Prog. Met. Phys. 6 (1956) 74–134.
[9] G.F. Vander Voort, A. Roósz, Metallography 17 (1984) 1–17.